Available online at www.sciencedirect.com
ScienceDirect
Dyes and Pigments 76 (2008) 477–484
DYES and PIGMENTS
www.elsevier.com/locate/dyepig

The enhancement of adsorption and photocatalytic activity of rare earth ions doped TiO_2 for the degradation of Orange I

Chun-Hua Liang [b], Fang-Bai Li [a,*], Cheng-Shuai Liu [a], Jia-Long Lü [b], Xu-Gang Wang [b]

[a] *Guangdong Key Laboratory of Agricultural Environment Pollution Integrated Control, Guangdong Institute of Eco-Environment and Soil Sciences, Guangzhou 510650, China*
[b] *College of Resources and Environmental Sciences, Northwest Agriculture and Forestry University, Yangling, Shaanxi 712100, China*

Received 27 July 2006; accepted 9 October 2006
Available online 13 November 2006

Abstract

Rare earth ions (Sm^{3+}, Nd^{3+}, Pr^{3+}) doped TiO_2 (RE^{3+}–TiO_2) catalysts were prepared by the sol–gel method, and characterized by X-ray diffraction (XRD) and diffuse reflectance spectroscopy (DRS). The adsorption abilities and photocatalytic activities of RE^{3+}–TiO_2 were evaluated by isothermal adsorption and Orange I degradation under UV light and visible light illumination. The adsorption results showed that RE^{3+}–TiO_2 had higher saturated adsorption amounts and higher adsorption equilibrium constants than pure TiO_2. The adsorption equilibrium constants (K_a) and the saturated adsorption amount (Q_{max}) of RE^{3+}–TiO_2 would increase with the increase of dosage. In the meantime, the photocatalytic activity of RE^{3+}–TiO_2 for Orange I degradation under both UV and visible light irradiations were higher than that of TiO_2. The optimal dosage was 1.5% for Orange I degradation under UV light and 1.0% under visible light. The higher photoactivity might be attributable to the transitions of 4f electrons of RE^{3+}.

Keywords: Photodegradation; Rare earth ion; Orange; Adsorption; TiO_2

1. Introduction

Like many other industrial effluents, wastewater in the textile industry had increased significantly recently in quantity in China that now poses a problem in terms of both biodegradability and toxicity. As textile wastewater is strongly colored which creates environmental and aesthetic problems [1], the contamination of water courses has become an issue of worldwide concern. In recent years, TiO_2 photocatalysis has been extensively studied due to its potential application for complete mineralization of many toxic and non-biodegradable organic pollutants [2–5]. However, modification of TiO_2 is necessary to enhance the efficiency of TiO_2 photocatalysis and to improve the photocatalytic activity of TiO_2 under solar or visible light [6,7]. To reduce the recombination of photogenerated electrons and holes on TiO_2, and also to extend its light absorption into the visible region, titanium dioxide has been doped with various transition metal ions [8–13]. Choi et al. [11] systematically studied 21 transition metal ions doped TiO_2 and found that when Fe^{3+}, Mo^{5+}, Ru^{3+}, Os^{3+}, Re^{5+}, V^{4+}, or Rh^{3+} were used at 0.1–0.5%, a significant increase in the photo-reactivity of TiO_2 was achieved for both chloroform oxidation and reduction. As the rare earth ions (RE^{3+}) can offer the advantage of transitions in the visible region, numerous studies of RE^{3+} ions in recent years have been focused on the luminescence properties of rare earth elements hosted in crystalline matrices [14–17]. On the basis of these properties, researchers have begun to pay attention to RE^{3+} doping of TiO_2 [18–24]. Some studies indicated that the photocatalytic activity of TiO_2 can be significantly enhanced by doping with lanthanide ions/oxides with 4f electron configurations, as lanthanide ions form complexes with various Lewis

* Corresponding author. Tel.: +86 20 87024721; fax: +86 20 87024123.
E-mail address: cefbli@soil.gd.cn (F.-B. Li).

0143-7208/$ - see front matter © 2006 Elsevier Ltd. All rights reserved.
doi:10.1016/j.dyepig.2006.10.006

bases including organic acids, amines, aldehydes, alcohols, and thiols by the interaction of the functional groups with their f-orbital [19,20]. Our group [18] reported the photocatalytic activity of Ce^{3+}–TiO_2, and proposed that the formation of two sub-energy levels (defect level and Ce 4f level) in Ce^{3+}–TiO_2 might be a key reason to eliminate the recombination of electron–hole pairs and to enhance the photocatalytic activity. Zhang et al. [21] reported the microstructure and photocatalytic properties of lanthanide doping of nanocrystalline mesoporous titanium dioxide and the results indicated that lanthanide doping could inhibit phase transformation from anatase to rutile, and the inhibitory effect was enhanced with the increase of the rare earth radius. Xie and Yuan [23] reported that Nd^{3+}–TiO_2 sol catalysts had higher photocatalytic activity for phenol degradation under visible light irradiation.

A systemic study of the photocatalytic properties and activity of TiO_2 doped with rare earth ions of different 4f electron configurations is necessary in order to investigate the dependence of activity on 4f electron configuration. In this context, this paper describes the preparation of three series of catalysts including Nd^{3+}–TiO_2, Sm^{3+}–TiO_2, Pr^{3+}–TiO_2, by the sol–gel method, and their photocatalytic activity and adsorption properties were investigated; Orange I was selected as a model chemical.

2. Experimental

2.1. Materials

Orange I was purchased from the Special Chemical Corporation of Shanghai, China and used without further purification. The pure TiO_2 and rare earth ion-doped TiO_2 catalysts were prepared with the raw materials of analytical grade. The raw materials included tetra-*n*-butyl titanium [Ti(O-Bu)$_4$], $Pr(NO_3)_3$, $Sm(NO_3)_3$, $Er(NO_3)_3$, acetic acid (99.8%), absolute ethanol and ethanol (95%) which were purchased from Aldrich and used without purification. Deionized water was used for preparing solutions in the experiments.

2.2. Preparation of catalysts

Catalysts were prepared by the sol–gel method with the following procedure: firstly, 17 mL of tetra-*n*-butyl titanium (Ti(O-Bu)$_4$) was dissolved in 80 mL of absolute ethanol; and then the Ti(O-Bu)$_4$ solution was added dropwise under vigorous stirring to 100 mL of the mixture solution containing 84 mL of ethanol (95%), 1 mL of 0.1 mol/L $RE(NO_3)_3$ ($Pr(NO_3)_3$, $Sm(NO_3)_3$, and $Er(NO_3)_3$), and 15 mL of acetic acid (>99.8%), and the resulting transparent colloidal suspension was stirred for 2 h before being aged for 2 days till the formation of gel. The gel was dried at 80 °C under vacuum and then ground into powder. The powder was calcined at 500 °C for 2 h and the product RE^{3+}–TiO_2 powder catalyst was eventually obtained in a nominal atomic doping level of 0.5%, named as 0.5% RE^{3+}–TiO_2. Accordingly, other RE^{3+}–TiO_2 samples containing different rare earth ion contents were named as 1.0% RE^{3+}–TiO_2, 1.5% RE^{3+}–TiO_2, and 2.0% RE^{3+}–TiO_2, respectively. Pure TiO_2 was prepared without addition of $RE(NO_3)_3$ in the procedure.

2.3. Characterization

The crystal phase of the powers were analyzed by X-ray power diffraction (XRD) using a Rigaku D/max 2500 diffractometer using Cu Kα radiation; the accelerating voltage was 40 kV and the emission current was 100 mA. To study the optical absorption of the catalysts, the diffuse reflectance spectra (DRS) of the catalysts in the wavelength range of 200–900 nm were obtained using a UV–vis reflectance spectrophotometer (Shimadzu UV-2101PC), with $BaSO_4$ as a reference.

2.4. Adsorption of Orange I in dark

To investigate the adsorption behavior of pure TiO_2 and RE^{3+}–TiO_2 catalysts, a set of adsorption isotherm tests were performed in the dark. A fixed amount of the adsorbent (0.1 g) was added to 10 mL of Orange I solution of varying concentrations taken in stoppered glass tubes, which were agitated for 24 h at 180 rpm in a thermostatic shaker bath and maintained at a temperature of 25 ± 1 °C until equilibrium was reached. At time $t = 0$ and equilibrium, the Orange I concentrations of the solutions were measured by UV–vis spectrometer and the adsorbed amount of Orange I on pure TiO_2 or RE^{3+}–TiO_2 catalysts were calculated based on a mass balance.

2.5. Photocatalytic activity evaluation

A Pyrex cylindrical photo-reactor was used to conduct photocatalytic oxidation experiments, in which an 8-W UVA lamp (Westbury, New York) with a special emission peak at 365 nm was positioned at the centre of the cylindrical vessel and was used for photoreaction under UV irradiation, while a 70-W high-pressure sodium lamp (Shanghai, China) with main emission in the range of 400–800 nm was used for photoreaction under visible light irradiation. This cylindrical photo-reactor was surrounded by a Pyrex circulating water jacket to control the temperature during the reaction. The reaction suspension was prepared by adding 0.25 g of RE^{3+}–TiO_2 powder into 250 mL of aqueous Orange I solution, the initial concentration of Orange I was 0.06 mmol/L. Prior to photoreaction, the suspension was magnetically stirred in the dark for 30 min to reach adsorption/desorption equilibrium. The aqueous suspension containing Orange I and RE^{3+}–TiO_2 power was aerated with a constant air flow to provide oxygen and for complete mixing of reaction solution. At the given time intervals, the analytical samples were taken from the suspension and immediately centrifuged at 4500 rpm for 30 min, and then its absorbance was determined at 481 nm to calculate its concentration.

2.6. Analytic method

To measure Orange I concentration of centrifuged samples, a UV–vis absorption spectrophotometer (UV–vis TU-1800, Purkinje General, Beijing) was used to determine the absorbance of Orange I at a wavelength of 481 nm. The absorbance set at 481 nm is due to the color of the dye solution and it is used to monitor the degradation of dye. The total organic carbon (TOC) concentration was determined using a Total Organic Analyzer instrument (Shimadzu TOC-V CPH).

3. Results and discussion

3.1. X-ray diffraction analyses of catalysts

Fig. 1 shows the XRD patterns of pure TiO_2 and RE^{3+}–TiO_2 powders from which it is clear that all catalysts were dominated by the anatase structure and the relative intensity of 101 peaks were broadened and reduced by rare earth ion doping. When the crystallite sizes of the RE^{3+}–TiO_2 samples were calculated using the Scherrer formula, it was found that the crystallite size was reduced by rare earth ion doping (Table 1). From Table 1, it is also apparent that there was no obvious difference between pure TiO_2 and RE^{3+}–TiO_2 powders in terms of the lattice parameters '*a*' and '*c*' which indicates that rare earth ions do not enter the lattice of anatase. It was concluded that rare earth ion doping could hinder crystal transformation and decrease crystallite size; generally, smaller crystalline size could lead to larger surface area [25].

3.2. Diffuse reflection spectra (DRS)

To study the optical absorption properties of catalysts, diffuse reflectance spectra (DRS) in the range of 200–900 nm were investigated (Fig. 2) from which it is evident that pure TiO_2 had no adsorption in the visible light region (>400 nm) whereas 1.5% Pr^{3+}–TiO_2 catalyst displayed a wide absorption band in the range 400–600 nm. The broad bands at 400–500 nm can be ascribed to f → f transition while the weak adsorption peak at around 600 nm was ascribed to the characteristic transition of $Pr^{3+1}D_2 \rightarrow {}^3H_4$ [26]. 1.5% Nd^{3+}–TiO_2 catalyst had four typical absorption peaks located at 527, 586, 762 and 809 nm, which corresponded to transitions of $^4I_{9/2}$ to $^2K_{13/2}$ and $^4G_{7/2}$, $^2G_{7/2}$ and $^4G_{5/2}$, $^4S_{3/2}$ and $^4F_{7/2}$, $^4F_{5/2}$ and $^2H_{9/2}$, respectively [16]. In the case of 1.5% Sm^{3+}–TiO_2 catalyst, whether in the UV region or visible region, the optical absorption was enhanced even though there was no obvious absorption peak.

Table 1
The crystal structure, crystal sizes, lattice parameter, and 101 peak relative intensity of different catalysts

Ion dosage (1.5%)	Pure TiO_2	Nd^{3+}–TiO_2	Sm^{3+}–TiO_2	Pr^{3+}–TiO_2
Crystal structure	Anatase	Anatase	Anatase	Anatase
Crystallite size (nm)	30.3	13.3	17.3	15.7
Lattice parameter *a* (nm)	0.380	0.381	0.380	0.382
Lattice parameter *c* (nm)	0.956	0.964	0.954	0.954
101 peak relative intensity (a.u.)	473	322	352	316

3.3. Adsorption behavior

Adsorption of pollutants on the semiconductor surface is an important parameter in heterogeneous photocatalysis. A set of isothermal adsorption experiments were carried out to evaluate the adsorption equilibrium constants and the extent of saturated adsorption. The isothermal adsorption curves of Orange I on different catalysts are shown in Fig. 3(A)–(C). The adsorption equilibrium constants (K_a) and the maximum saturated adsorption (Q_{max}) obtained from the adsorption experiments were fitted to the linear form of the rearranged Langmuir equation as follows:

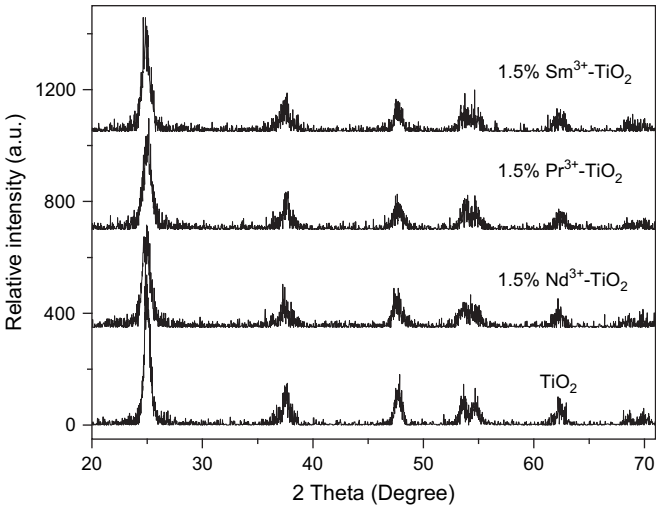

Fig. 1. The XRD patterns of TiO_2 and 1.5% RE^{3+}–TiO_2 catalyst powders.

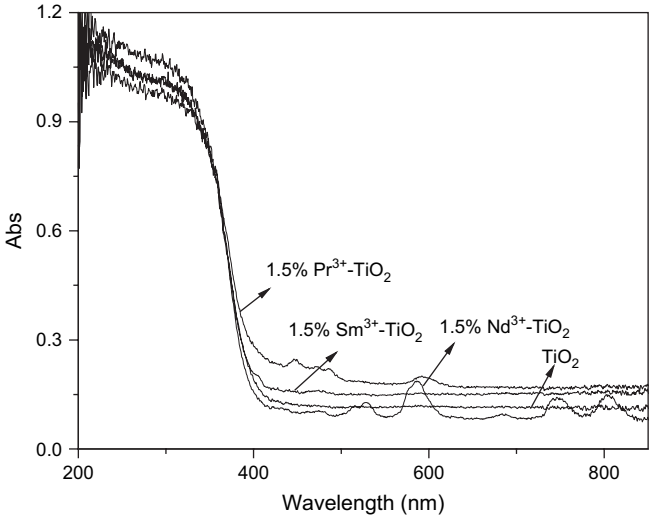

Fig. 2. The UV–vis diffuse reflectance spectra of TiO_2 and 1.5% RE^{3+}–TiO_2 catalysts.

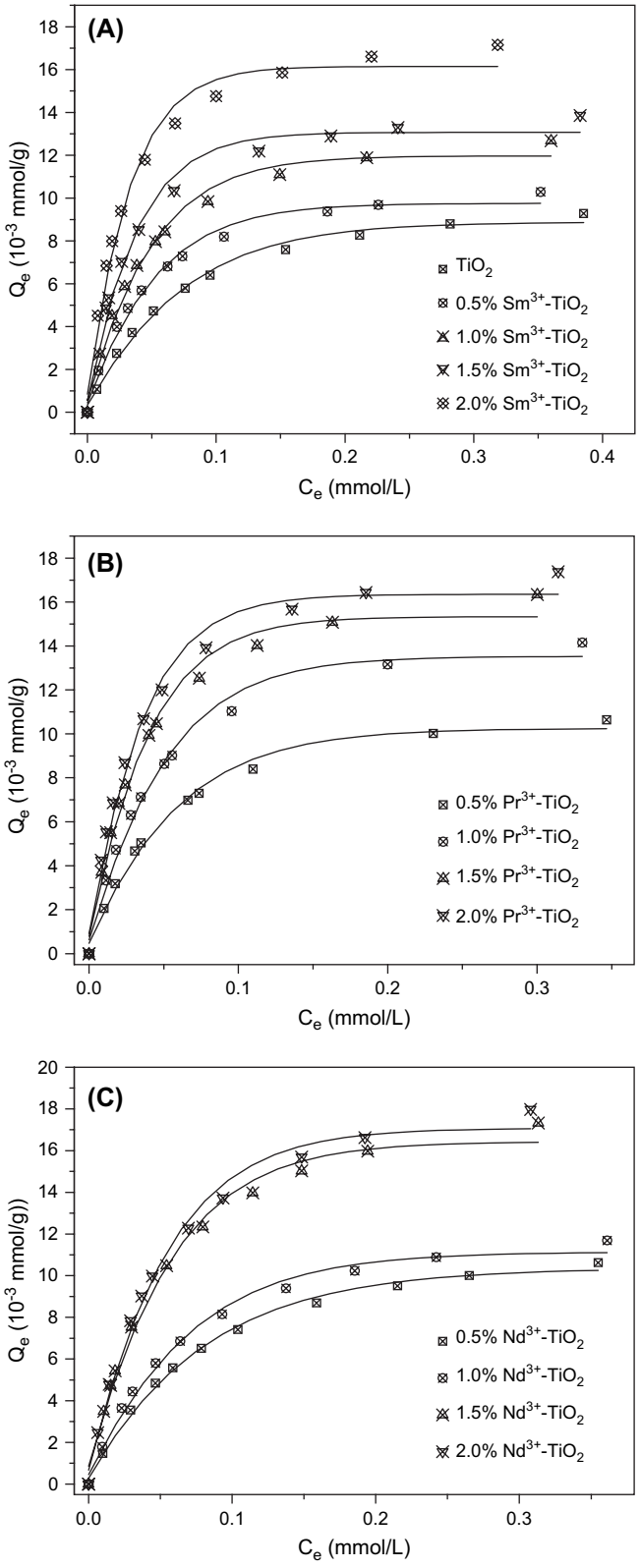

Fig. 3. Adsorption isotherms of Orange I on TiO_2 and RE^{3+}–TiO_2 catalyst powders in dark.

$$\frac{C_e}{Q_e} = \frac{1}{K_a Q_{max}} + \frac{C_e}{Q_{max}} \quad (1)$$

A plot of C_e/Q_e versus C_e furnished a straight line and the Langmuir adsorption parameters were obtained from the slope and intercept of the line (Table 2) from which it is clear that the adsorption equilibrium constants (K_a) and the maximum saturated adsorption (Q_{max}) of Orange I in all RE^{3+}–TiO_2 samples were greater than that for pure TiO_2, whose K_a was 14.96×10^3 L/mol and Q_{max} was 10.89×10^{-6} mol/g. Of the RE^{3+}–TiO_2 photocatalysts, 2.0% Nd^{3+}–TiO_2 showed the highest maximum saturated adsorption (Q_{max} of 20.94×10^{-6} mol/g) and 2.0% Sm^{3+}–TiO_2 had the highest adsorption equilibrium constant ($K_a = 39.33 \times 10^3$ L/mol). The K_a and Q_{max} on the RE^{3+}–TiO_2 catalysts increased with the increase of rare earth ion content.

3.4. Evaluation of photocatalytic activity

The photocatalytic activity of three series of TiO_2 catalysts doped with rare earth ions were evaluated under UV light and visible light. A set of experiments were conducted with 1.0 g/L RE^{3+}–TiO_2 and 0.06 mM Orange I under UV light irradiation as shown in Fig. 4 and visible light as shown in Fig. 5. The degradation of Orange I could be described by first-order kinetic of $-\ln(C_t/C_0)$ versus reaction time (t):

$$-\ln\frac{C_t}{C_0} = k_{ap} t \quad (2)$$

where k_{ap} is the apparent reaction rate constant, and C_0 and C_t are the initial concentration and the concentration of Orange I at reaction time t, respectively. From Figs. 4(A) and 5(A), we can see that the photocatalytic activity of samarium ion-doped TiO_2 was significantly higher than that of pure TiO_2 under both UV light and visible light. The photocatalytic activity increased with increasing the Sm^{3+} dosage initially, but decreased when Sm^{3+} doping content was over an optimal dosage. Obviously, 1.5% Sm^{3+}–TiO_2 achieved the best photocatalytic performance with k_{ap} of 6.92×10^{-2} min^{-1} under UV light irradiation and 1.0% Sm^{3+}–TiO_2 achieved the best photocatalytic performance with k_{ap} of 2.96×10^{-2} min^{-1} under visible light. Similar results could be obtained for Pr^{3+}–TiO_2 catalysts and Nd^{3+}–TiO_2 catalysts with which 1.5% RE^{3+} content has the highest photocatalytic activities under UV light irradiation and 1.0% RE^{3+} content achieved the best photocatalytic performance under visible light irradiation, as shown in Fig. 4(B) and (C) and Fig. 5(B) and (C). The first-order constants and relative coefficients are shown in Table 3. From Table 3, it could be seen that the photocatalytic activities of RE^{3+}–TiO_2 under visible light were also enhanced significantly compared with that of pure TiO_2 (1.55×10^{-2} min^{-1}). The photocatalytic activity of RE^{3+}–TiO_2 for Orange I degradation under both UV light and visible light irradiation enhanced with the increase of RE^{3+} doping content initially, but decreased while the RE^{3+} content reached a higher level.

Table 2
Langmuir adsorption equilibrium constant ($K_a \times 10^3$ L/mol) and saturated adsorption amount ($Q_{max} \times 10^{-6}$ mol/g) for Orange I on catalysts

Dosage (%)	Sm^{3+}–TiO_2			Pr^{3+}–TiO_2			Nd^{3+}–TiO_2		
	K_a	Q_{max}	R^2	K_a	Q_{max}	R^2	K_a	Q_{max}	R^2
0	14.96	10.89	0.979						
0.5	23.07	11.55	0.988	20.41	12.15	0.984	12.88	12.94	0.966
1.0	24.54	14.12	0.989	23.29	16.00	0.95	15.56	13.77	0.993
1.5	33.31	14.95	0.995	30.20	18.15	0.942	20.04	20.80	0.943
2.0	39.33	18.52	0.995	35.36	18.94	0.977	20.74	20.94	0.970

Generally, pure TiO_2 cannot be excited by visible light. From Table 3, it could also be seen that the pure TiO_2 showed photocatalytic activity, due to dye sensitization, which led to photocatalytic activity of pure TiO_2 as presented in Eqs. (3)–(8)

$$\text{Dye} + h\nu \rightarrow \text{dye}^* \quad (3)$$

$$TiO_2 + \text{dye}^* \rightarrow TiO_2(e^-) + \text{dye}^{+\bullet} \quad (4)$$

$$O_2 + TiO_2(e^-) \rightarrow O_2^{-\bullet} + TiO_2 \quad (5)$$

$$O_2^{-\bullet} + H_2O \rightarrow HO_2^{\bullet} + OH^- \quad (6)$$

$$HO_2^{\bullet} + H_2O + TiO_2(e^-) \rightarrow H_2O_2 + OH^- + TiO_2 \quad (7)$$

$$H_2O_2 + TiO_2(e^-) \rightarrow OH^{\bullet} + OH^- + TiO_2 \quad (8)$$

3.5. Mineralization

For the purpose of contaminant control in the degradation process, it is desirable to mineralize the organic pollutants into CO_2 and H_2O. Accordingly, we carried out a series of experiments of mineralization under UV light irradiation by using pure TiO_2 and 1.5% RE^{3+}–TiO_2. The results in Fig. 6 indicated that Orange I mineralization was efficiently enhanced owing to rare earth ion doping. The percentage of TOC removal was 82.8%, 99.7%, 97.4% and 86.6% in the suspension of pure TiO_2, 1.5% Sm^{3+}–TiO_2, 1.5% Pr^{3+}–TiO_2 and 1.5% Nd^{3+}–TiO_2, respectively, after 150 min UV light irradiation. The mineralization efficiency was in the order of rare earth doped with 1.5% Sm^{3+}–TiO_2 > 1.5% Pr^{3+}–TiO_2 > 1.5% Nd^{3+}–TiO_2 > pure TiO_2, which was in good agreement with that of the first-order rate constants.

3.6. Discussion

The ionic radii of Sm^{3+}, Nd^{3+}, and $Pr^{3+}$are 0.96, 0.99, and 1.01 Å, respectively, which are much larger than that of Ti^{4+} (0.68 Å). There was no obvious difference of the lattice parameter '*a*' and '*c*' between the pure TiO_2 and RE^{3+}–TiO_2 powders from XRD analysis (Table 1), which indicated that these rare earth ions could not enter into the lattice of TiO_2 to replace the Ti^{4+} ion. Xu et al. [27] proposed that rare earth salts were changed to rare earth oxides during the calcination processing, and these oxides were uniformly adsorbed on the surface of TiO_2 and may favor separating the charge carriers efficiently. Moreover, Ti^{4+} ion could be substituted by rare earth ions in the lattice of rare earth oxide to form tetrahedral Ti sites, which created a charge imbalance, so more hydroxide ions would be adsorbed on the surface for charge balance. These hydroxide ions on the surface can accept holes generated by UV irradiation to form hydroxyl radicals [27]. Therefore, the photo-induced charge carrier recombination can be restrained. DRS spectra of RE^{3+}-doped TiO_2 catalysts showed that there were optical adsorption in visible region and red shifts in the RE^{3+}-doped TiO_2, which is ascribed to the transitions of 4f electrons of RE^{3+}.

It is well known that the photocatalytic activity strongly depend on the better adsorption of organic substrate and the improvement of the interfacial charge transfer reaction [27,28]. Interfacial charge transfer is possible only when the donor or acceptor is pre-adsorbed before the photocatalytic reaction. The preliminary adsorption of the substrates and the amount of adsorption are very important pre-requisites for highly efficient degradation. From Section 3.3, we can know that all doping catalysts showed the stronger adsorption capacities than pure TiO_2. The factors leading to the enhanced adsorption capacity should involve the change of the physical or chemical properties of the catalysts owing to rare earth ion doping. The smaller crystal size and larger specific surface area of RE^{3+}–TiO_2 catalysts would be beneficial to achieve better physical adsorption of Orange I in the aqueous suspensions. Moreover, it was reported that lanthanide ions could complex with azo dyes to form solid complexes [29,30]. Thus, there might be another important enhancement for the adsorption of Orange I on RE^{3+}–TiO_2 by forming a chemical complex of RE^{3+} and Orange I in the aqueous suspension. The transitions of 4f electrons of RE^{3+} led to the enforcement of the optical adsorption of catalysts and favored the separation of photo-generated electron–hole pairs. In addition, the red shift of the optical adsorption edge of TiO_2 by rare earth ion doping was helpful to the improvement of visible light photocatalytic activity of TiO_2. Therefore, the transitions of 4f electrons of RE^{3+} and red shifts of the optical adsorption edge of TiO_2 by rare earth ion doping and dye sensitization enhanced visible light photocatalytic activity of TiO_2.

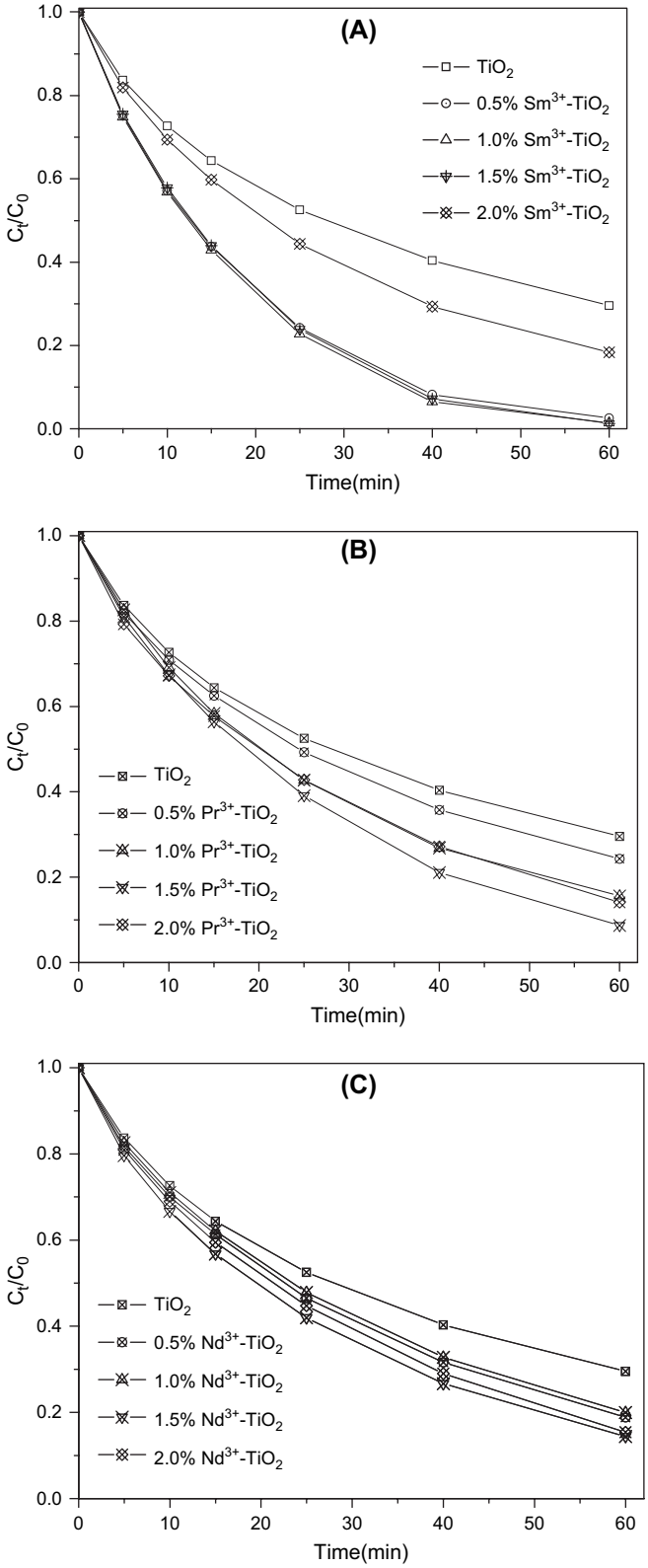

Fig. 4. The degradation of 0.06 mM Orange I on TiO_2 and RE^{3+}–TiO_2 catalyst powders under UV light (pH = 6.86, catalyst dosage = 1.0 g/L).

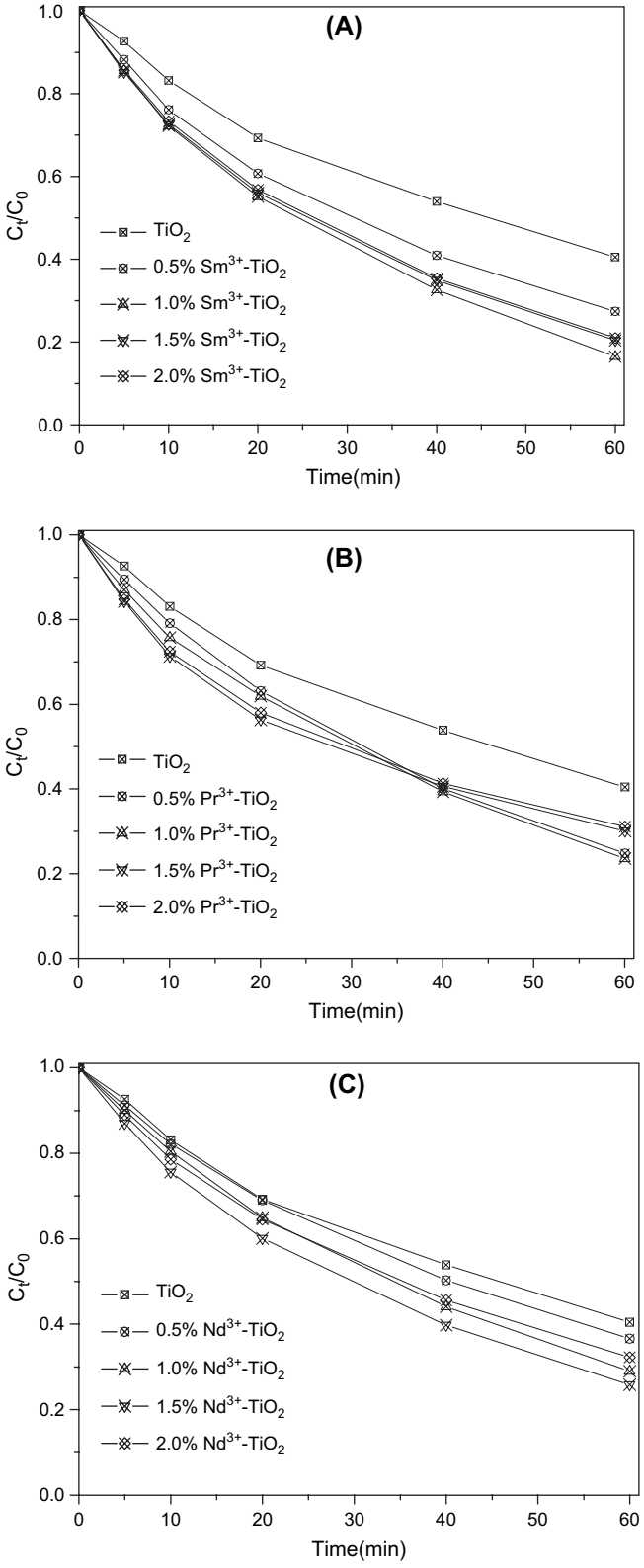

Fig. 5. The degradation of 0.06 mM Orange I on TiO_2 and RE^{3+}–TiO_2 catalyst powders under visible light (pH = 6.86, catalyst dosage = 1.0 g/L).

The optimal dosage of rare earth ions at 1.5% for Orange I degradation under UV irradiation and at 1.0% under visible light irradiation in this study might be contributed to the fact that there was an optimal dosage of rare earth ions in TiO_2 particles for the most efficient separation of photo-induced electron–hole pairs. As the content of doping ions increases, the surface barrier becomes higher, and the space charge region becomes narrower. The electron–hole pairs

Table 3
The first-order kinetic constants (k_{ap}, min^{-1}) and relative coefficient (R^2) for degradation of Orange I under both UV light and visible light irradiations

Dosage (%)	Sm^{3+}–TiO_2				Pr^{3+}–TiO_2				Nd^{3+}–TiO_2			
	UV light		Visible light		UV light		Visible light		UV light		Visible light	
	k_{ap}	R^2	k_{ap}	R^2	k_{ap}	R^2	k_{ap}	R^2	k_{ap}	R^2	k_{ap}	R^2
0	0.0221	0.989	0.0155	0.992								
0.5	0.0611	0.997	0.0222	0.994	0.0251	0.974	0.0231	0.999	0.0280	0.990	0.0171	0.997
1.0	0.0689	0.990	0.0296	0.998	0.0321	0.994	0.0239	0.998	0.0285	0.994	0.0230	1.000
1.5	0.0692	0.983	0.0268	0.996	0.0399	0.998	0.0216	0.952	0.0316	0.996	0.0207	0.995
2.0	0.0298	0.988	0.0264	0.997	0.0331	0.995	0.0210	0.957	0.0315	0.997	0.0194	0.993

within the region are efficiently separated by the large electric field before recombination which led to the higher photocatalytic activity. However, when the content of doping ions is excessively high, the space charge region becomes very narrow and the penetration depth of light into TiO_2 greatly exceeds the space charge layer; therefore the recombination of the photo-generated electron–hole pairs becomes easier, which led to the lower photocatalytic activity of TiO_2 for Orange I degradation. Therefore, there was an optimal RE^{3+} doping for Orange I degradation under both UV and visible light irradiations.

4. Conclusions

Rare earth ion (Sm^{3+}, Nd^{3+}, Pr^{3+}) doping in TiO_2 could enhance the saturated adsorption amount and adsorption equilibrium constants, and also increase the photocatalytic activity for the degradation of Orange I. The increase in photocatalytic activity was due to the higher adsorption, and the 4f electron transition of RE^{3+}. The highest photoactivity was obtained at 1.5% RE^{3+} dosage under UV light irradiation, and at 1.0% RE^{3+} dosage under visible light.

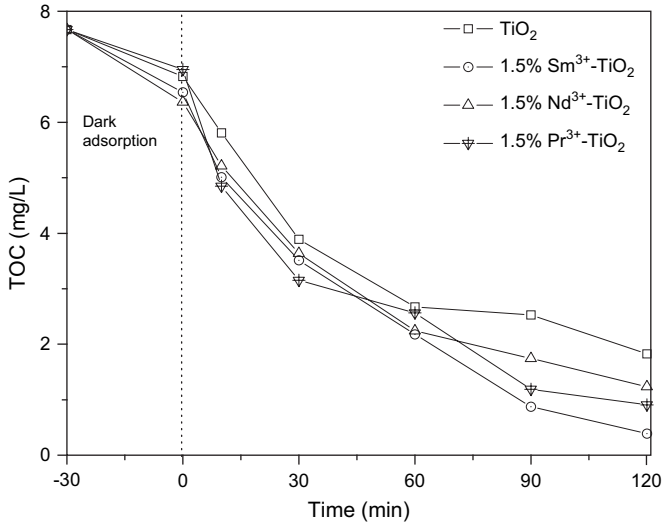

Fig. 6. The removal percentage of total organic carbon versus time under UV light irradiation (0.06 mM Orange I, pH = 6.86, catalyst dosage = 1.0 g/L).

Acknowledgements

The authors would like to thank the National Natural Science Foundation of China (No. 20377011), Foundation of Natural Science of Guangdong Province (No. 031293) and Guangdong Technological Foundation (No. 2005B10301001) for financial supports to this work.

References

[1] Alaton IA, Balciglu IA, Bahnemann DW. Advanced oxidation of a reactive dye bath effluent: comparison of O_3, H_2O_2/UV-C and TiO_2/UV-A processes. Water Res 2002;36:1143–54.
[2] Fujishima A, Rao TN, Tryk DA. Titanium dioxide photocatalysis. J Photochem Photobiol C Photochem Rev 2000;1:1–21.
[3] Hoffmann MR, Martin ST, Choi W, Bahnemann DW. Environmental applications of semiconductor photocatalysis. Chem Rev 1995;95:69–96.
[4] Muruganandham M, Swaminathan M. Photo-catalytic decolourisation and degradation of Reactive Orange 4 by TiO_2–UV process. Dyes Pigments 2006;68:133–42.
[5] Li XZ, Li FB. Study of Au/Au^{3+}–TiO_2 photocatalysts toward visible photooxidation for water and wastewater treatment. Environ Sci Technol 2001;35:2381–7.
[6] Bae E, Choi W. Highly enhanced photoreductive degradation of perchlorinated compounds on dye-sensitized metal/TiO_2 under visible light. Environ Sci Technol 2003;37:147–52.
[7] Li XZ, Li FB, Yang CL, Ge WK. Photocatalytic activity of WO_x–TiO_2 under visible light irradiation. J Photochem Photobiol A Chem 2001;141:209–17.
[8] Yu JG, Yu JC, Leung MKP, Ho WK, Cheng B, Zhao XJ, et al. Effects of acidic and basic hydrolysis catalysts on the photocatalytic activity and microstructures of bimodal mesoporous titania. J Catal 2003;217:69–78.
[9] Yu JG, Yu HG, Cheng B, Zhao XJ, Yu JC, Ho WK. The effect of calcination temperature on the surface microstructure and photocatalytic activity of TiO_2 thin films prepared by liquid phase deposition. J Phys Chem B 2003;107:13871–9.
[10] Paola AD, Marci G, Palmisano L, Schiavello M, Uosaki K, Ikeda S, et al. Preparation of polycrystalline TiO_2 photocatalysts impregnated with various transition metal ions: characterization and photocatalytic activity for the degradation of 4-nitrophenol. J Phys Chem B 2002;106:637–45.
[11] Choi W, Termin A, Hoffmann MR. The role of metal ion dopants in quantum-sized TiO_2: correlation between photoreactivity and charge carrier recombination dynamics. J Phys Chem 1994;98:13669–79.
[12] Wang JA, Limas-Ballesteros R, Lopez T, Moreno A, Gomez R, Novaro OX, et al. Quantitative determination of titanium lattice defects and solid-state reaction mechanism in iron-doped TiO_2 photocatalysts. J Phys Chem B 2001;105:9692–8.
[13] Jin S, Shiraishi F. Photocatalytic activities enhanced for decompositions of organic compounds over metal-photodepositing titanium dioxide. Chem Eng J 2004;97:203–11.

[14] Zhu J, Zhu K, Chen L. Influence of gold nanoparticles on the up-conversion fluorescence in Sm^{3+}. J Non-Cryst Solids 2006;352:150–4.
[15] Gacon JC, Horchani K, Jouini A, Dujardin C, Kamenskikh I. Optical properties of praseodymium concentrated phosphates. Opt Mater 2006;28:14–20.
[16] Koepke Cz, Wisniewski K, Sikorski L, Piatkowski D, Kowalska K, Naftaly M. Upconverted luminescence under 800 nm laser diode excitation in Nd^{3+}-activated fluoroaluminate glass. Opt Mater 2006;28:129–36.
[17] Philip L, Christiane GW, Koen B. Luminescent europium(III) and terbium(III) nicotinate complexes covalently linked to a 1,10-phenanthroline functionalised sol–gel glass. J Lumin 2006;117:163–9.
[18] Li FB, Li XZ, Hou MF, Cheah KW, Choy WCH. Enhanced photocatalytic activity of Ce^{3+}–TiO_2 for 2-mercaptobenzothiazole degradation in aqueous suspension for odour control. Appl Catal A Gen 2005;285:181–9.
[19] Ranjit KT, Willner I, Bossmann SH, Braun AM. Lanthanide oxide doped titanium dioxide photocatalysts: effective photocatalysts for the enhanced degradation of salicylic acid and *t*-cinnamic acid. J Catal 2001;204:305–13.
[20] Ranjit KT, Willner I, Bossmann SH, Braun AM. Lanthanide oxide-doped titanium dioxide photocatalysts: novel photocatalysts for the enhanced degradation of *p*-chlorophenoxyacetic acid. Environ Sci Technol 2001; 35:1544–9.
[21] Zhang YH, Zhang HX, Xu YX, Wang YG. Significant effect of lanthanide doping on the texture and properties of nanocrystalline mesoporous TiO_2. J Solid State Chem 2004;177:3490–8.
[22] Li FB, Li XZ, Hou MF. Photocatalytic degradation of 2-mercaptobenzothiazole in aqueous La^{3+}–TiO_2 suspension for odor control. Appl Catal B Environ 2004;48:185–94.
[23] Xie YB, Yuan CW. Photocatalysis of neodymium ion modified TiO_2 sol under visible light irradiation. Appl Surf Sci 2004;221:17–24.
[24] Jeon S, Braun PV. Hydrothermal synthesis of Er-doped luminescent TiO_2 nanoparticles. Chem Mater 2003;15:1256–63.
[25] Hou MF, Li FB, Li RF, Wan HF, Zhou GY, Xie KC. Mechanisms of enhancement of photocatalytic properties and activity of Nd^{3+}-doped TiO_2 for Methyl Orange degradation. J Rare Earths 2004;22:542–6.
[26] Yan B, Zhou K. In situ sol–gel composition of inorganic/organic polymeric hybrid precursors to synthesize red-luminescent $CaTiO_3:Pr^{3+}$ and $CaTi_{0.5}Zr_{0.5}O_3:Pr^{3+}$ phosphors. J Alloys Compd 2005;398:165–9.
[27] Xu AW, Gao Y, Liu HQ. The preparation, characterization, and their photocatalytic activities of rare-earth-doped TiO_2 nanoparticles. J Catal 2002;207:151–7.
[28] Colombo DP, Bowman RM. Femtosecond diffuse reflectance spectroscopy of TiO_2 powders. J Phys Chem 1995;99:11752–6.
[29] Abdel-Ghani NT, El-Ansary AL, Salem AA. Thermogravimetric, potentiometric, conductimetric and spectrometric studies on lanthanide complexes with some hydroxynaphthoic acid azo dyes. Thermochim Acta 1987;122:231–43.
[30] Abdel-Ghani NT, Issa YM, Salem AA. Spectrophotometric determination of some lanthanides using 3-hydroxy-2-naphthoic acid azo dyes. Microchem J 1989;39:283–8.